MOLEKUL
eISSN: 2503-0310

Articles
https://doi.org/10.20884/1.jm.2023.18.2.7480

Effect of Annealing and Etching Times on Anatase TiO_2 Hollow Sphere

Khusna Arif Rakhman[1,2], Nurul Hidayat Aprilita[1], Indriana Kartini[1]*

[1]Department of Chemistry, Universitas Gadjah Mada, Yogyakarta, 55281, Indonesia
[2]Department of Chemistry Education, Khairun University, Ternate, 97728, Indonesia

*Corresponding author email: indriana@ugm.ac.id

Received December 21, 2022; **Accepted** May 05, 2023; **Available online** July 20, 2023

ABSTRACT. The development of high-efficiency photocatalysts plays an important role in the application of solar energy conversion. Titanium dioxide (TiO_2) with an anatase crystalline phase is well-known as semiconductor thin layers for solar cells. This work has constructed a novel TiO_2 hollow sphere (HST) in a 2-step synthesis. The first step is coating the SiO_2 template with TiO_2 to build a core-shell of SiO_2@TiO_2 (CSST). The second step is etching via sonication to elute the SiO_2 from CSST and construct the HST. The annealing of CSST for 1 to 6 hours and etching for 1 to 7 hours has resulted in the HST with different crystallite sizes and microstrains. The HST of ~90 nm has been fabricated with crystallite size of 9.53 to 20.54 nm and microstrain from 0.34 to 3.42. It was found that the optimum crystallite size and microstrain of HST obtained via annealing the CSST for 2 hours and etching for 5 hours has the best photooxidation of I^- under UV irradiation. The optimum crystallite size and microstrain of HST via annealing and etching times can be recommended for the future of solar cell fabrication and applications.

Keyword: Anatase TiO_2, annealing time, etching, hollow sphere TiO_2, photocatalytic activity

INTRODUCTION

In recent years, the architecture of hollow sphere TiO_2 (HST) has attracted particular attention in photocatalyst and solar cell applications because of the advantages of HST which have a wide band gap and incident light scattering (Fang et al., 2022). These characteristics are essential to enhancing the efficiency of the photocatalytic activity (Shakeel et al., 2017). Furthermore, the size of particles and cavities in HST also impacts the scattering of light of the photocatalysts, which can be advantageous in improving performance. The small size of HST makes a large surface area into a sizeable light-contact space (Liao et al., 2012). While the cavities of HST as this morphological uniqueness provide an extension of the wavelength to enhance the scattering effect (Jafarzadeh et al., 2016; Tsai et al., 2014). Those properties can be designed based on the HST fabrication.

HST fabrication has two synthesis pathways, namely hydrothermal and sol-gel. The hydrothermal synthesis of HST has a single step while sol-gel involves two steps. Hydrothermal was implemented in an autoclave at high temperatures (Wang et al., 2014), producing more than 100 nm HST of particle size (Zhu et al., 2013). Meanwhile, the sol-gel synthesis of HST began with the templating through core@shell formation and continued with removing the core to form HST (Choi et al., 2011). The sol-gel by carbon-based templates have fabricated HST with particle sizes between 60 and 365 nm (Choi et al., 2011) while using the SiO_2-based templates could produce 25-100 nm HST particle size (Chen et al., 2012; Oh et al., 2010).

Photocatalysts with smaller particles have large surface areas which enhance the contact area and scatter the incident light, thus increasing the photocatalytic activity. Consequently, the sol-gel method using the SiO_2 template is preferred for fabricating the HST because it can produce smaller particles compared to the hydrothermal method (Jeng et al., 2013). The HST fabrication begins with the formation of CSST by coating the SiO_2 template synthesized by the Stöber method with a TiO_2 precursor (Choi et al., 2011; Kim et al., 2010). The particle size, cavity, and shell thickness of HST can be designed at this step, while the anatase phase has been constructed after annealing of CSST at more than 500 °C (Kanjana et al., 2020; Oh et al., 2010; Li et al., 2013; Yao et al., 2020). Hence, an annealing process is an essential step to construct the anatase TiO_2. Zheng et al. (2018) have reported the optimum annealing temperature of CSST to construct anatase HST at 900 °C. The anatase HST constructed at 500 °C has the low peak of the XRD diffractogram and collapsed at 1100 °C. Yun et al. (2015) synthesized anatase HST at 6 hours of annealing at 900 °C. The appropriate annealing time in synthesizing TiO_2

nanoparticles enhances the crystallite size, dislocation density, microstrain, and oxygen vacancy responsible for the increased magnetic moment in TiO_2 nanoparticles (Doubi et al., 2019; Thejas et al., 2022). The annealing time also affects the optimum optical properties in the preparation of the TiO_2 nanoparticles (Tighineanu et al., 2010). The optimum microstrain and dislocation density showed a better adsorption performance (John et al., 2021). The optimum microstrain of anatase TiO_2 has also a high efficiency of photocatalytic activity. Therefore, to get the optimum microstrain, the optimization of annealing time has been studied to enhance the photocatalysis activity of HST.

Next, removing the SiO_2 core from CSST using an alkaline solution (etching process) is the second step to produce the HST. Sodium hydroxide (NaOH) solution was chosen because of its high selectivity to soluble SiO_2 (Choi et al., 2011; S. Li et al., 2013; Lyu et al., 2020). The NaOH solution in this process pushes high energy intensity into the voids between the silica-titania and causes partial etching of the SiO_2 core (Chen et al., 2012). The etching of SiO_2 by NaOH solution was reported at different times, 3 to 6 hours (Oh et al., 2010; Yun et al., 2015; Zheng et al., 2018). Meanwhile, the etching time is thought to affect the anatase HST microstrain after losing the SiO_2 core. To avoid concerns about changes in HST morphology because of microstrain changes from the impact of etching time, the etching time optimization is studied in this article to obtain the optimum etching time.

Time is our concern for the fabrication of anatase of HST, while the annealing and etching are the main steps to constructing the ones. Although the optimal annealing temperature of HST was reported, the annealing and etching times have not been studied previously. Generally, studies of HST as a photocatalyst have widely reported has superior morphology with unique pore characteristics and the ability to scatter light to enhance the efficiency of photocatalytic activity. Thus, in this work, we studied the effect of annealing and etching times to obtain the optimum crystallite size and microstrain of anatase HST. The photocatalytic activity of the anatase HST was determined using iodide ion (I^-) photooxidation. According to Li et al. (2013), photooxidation I^- mimics the process of electron regeneration in the redox electrolytes (I^-/I_3^-) of a DSSC system. Therefore, the photocatalytic activity of HST on this system can serve as an indicator of its performance when applied to DSSCs, much like the redox performance in the DSSC system.

EXPERIMENTAL SECTION

Synthesis of HST

All chemicals are of analytical grade quality without any further purification. The synthesis of HST began with the construction of the SiO_2 sphere by the Stöber method (Meier et al., 2018; Stober, 1968). Firstly, 3.6 mL of titanium(IV) isopropoxide (TTIP) (Merck) precursor was dissolved into 8 mL of ethanol (Merck). The solution was mixed with a solution of 6 mL of acetonitrile (Merck) and 10 mL of ethanol, then added to 30 mL of colloidal SiO_2 nanoparticles. The TTIP solution and SiO_2 were reacted by stirring via a sol-gel coating process for 6 hours above an ice bath. The colloid CSST formed was obtained by centrifuging and sequentially washing with ethanol and deionized water. The CSST was annealed at 900 °C for altered times: 0, 1, 2, 4, and 6 hours. The HST was etched by eluting the CSST in 2.5 M NaOH (Merck) solution with a weight-to-volume ratio of 1:4, then sonicating for time variations of 0, 1, 3, 5, and 7 hours.

Photocatalytic Activity

The photocatalytic activity of HST 1-6 (different of CSST annealing times 1-6 hours and after etching 5 hours) was analyzed based on the I_3^- formed from the photooxidation of I^- in 10 mL KI (Merck) 0.2 M and 50 mg of HST by stirring and irradiation at 25 cm under UV light (40 W, with a maximum emission at about 254 nm) at room temperature for 15, 30, 45 and 60 minutes. The suspension was centrifuged, then the supernatant was diluted 10 times. The absorbance of the solution was monitored by a UV/Vis Spectrophotometer (Thermo Scientific, Orion AquaMate 8100) at 288 nm (Pavasupree et al., 2006). The concentration of I_3^- was determined by Equation 1. In the dark and without the HST samples were observed no I_3^- formed.

$$A = \varepsilon.b.c \quad (1)$$

Where A: absorbance, a: the molar extinction coefficient 4.0×10^4 $(cm\ mol/L)^{-1}$, b: cuvette thickness, and c: concentration.

Characterization

The HST sample was characterized using transmission electron microscopy (TEM, JEOL: JEM-1400) and a field emission scanning electron microscope (FESEM, Quanta FEG-650). While the diffractograms of the crystallite phase of the sample were determined by X-ray diffraction (Shimadzu, XRD-6000) with a Cu Kα radiation source (λ = 1.5406) at 40 kV and 300 mA (12 W). Fourier transform infrared (FTIR, Shimadzu prestige 21) was used to identify the functional groups of the sample, and a UV/Vis Spectrophotometer (Shimadzu, UV-2401PC) determined the UV/Vis diffuse reflectance spectra. The SiO_2 loss via the etching process was monitored using an energy-dispersive X-ray spectrometer (EDS, JEOL JSM-6510LA).

RESULTS AND DISCUSSION

Synthesis of Hollow Sphere TiO_2

The fabrication of HST begins by preparing the surface of the SiO_2 template in a positive charge with an ammonia solution. The positive charge on the surface of SiO_2 by NH_4^+ drives the interaction with Ti-OH and constructs the CSST via the condensation

process at low temperatures (Kim et al., 2010); the SiO_2 template was then eluted by an etching process using sodium hydroxide solution to produce HST (S. Li et al., 2013; Lyu et al., 2020). An illustration of these reactions can be seen in **Figure 1.a.**

The morphology and structure of synthesized HST are presented in **Figure 1.b** to **1.e**. FESEM image (**Figure 1.b**) showed a SiO_2 template with a particle size of ~65 nm generated from the Stöber method. (d) CSST has an inner diameter of ~45 nm, with a shell thickness of ~25 nm. The SiO_2 template has shrunk after CSST construction and annealing at 900 °C because of the arrangement of the anatase TiO_2 (Yun et al., 2015). While **Figure 1.e** shows HST with a cavity of ~45 nm and a shell thickness of ~26 nm. The shell thickness of CSST and HST is supposed to be constant because there is no TiO_2 crystal etch in the etching process.

The functional groups in CSST and HST can be identified through the FTIR spectra (**Figure 2.a**). The Si-O-Ti peak was identified at 949 cm^{-1} in the SiO_2 template and SiO_2/TiO_2, as reported by Chang et al. (2017); Lewhie et al. (2007); and D. Wang et al. (2019) who found the peak at around 940-962 cm^{-1}. The synthesis of HST via CSST showed a weakening of the 949 cm^{-1} peak and claimed a change of Si-O-H to Si-O-Ti. The formation of Si-O-Ti bonds was strengthened by the redshift of 1.063 to 1.099 cm^{-1}, which indicated a decrease in frequency and vibrational energy or elongation of Si-O bonds. **Figure 2.b** shows an X-ray profile of CSST after annealing at 900 °C. The CSST and HST profiles consistently showed the anatase crystal structures, while the SiO_2/TiO_2 demonstrated the different crystal structures: (A) anatase and (R) rutile.

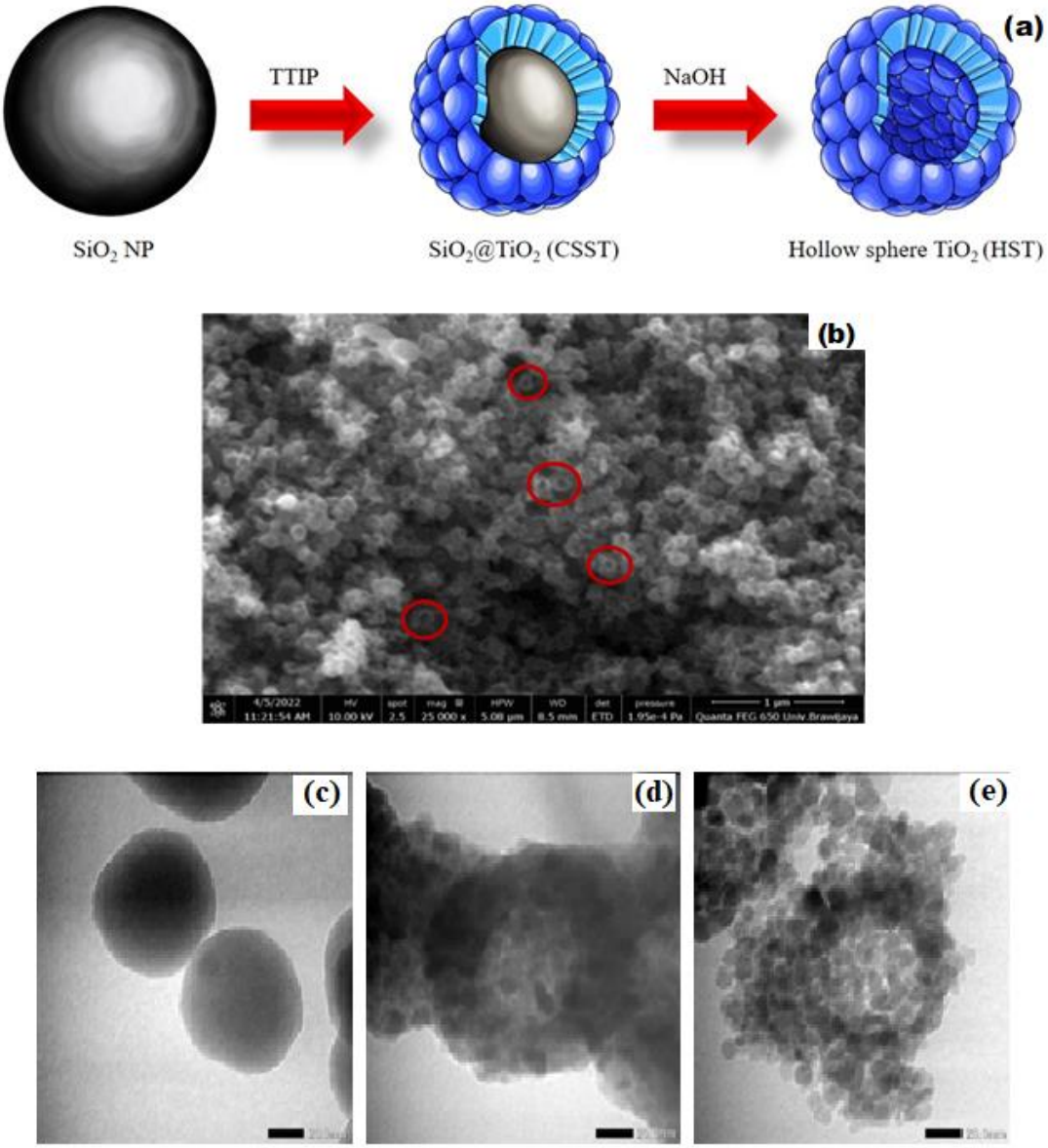

Figure 1. Image (**a**)-(**b**): FESEM and illustration of HST fabrication, (**c**)-(**e**) TEM: SiO_2, CSST, HST

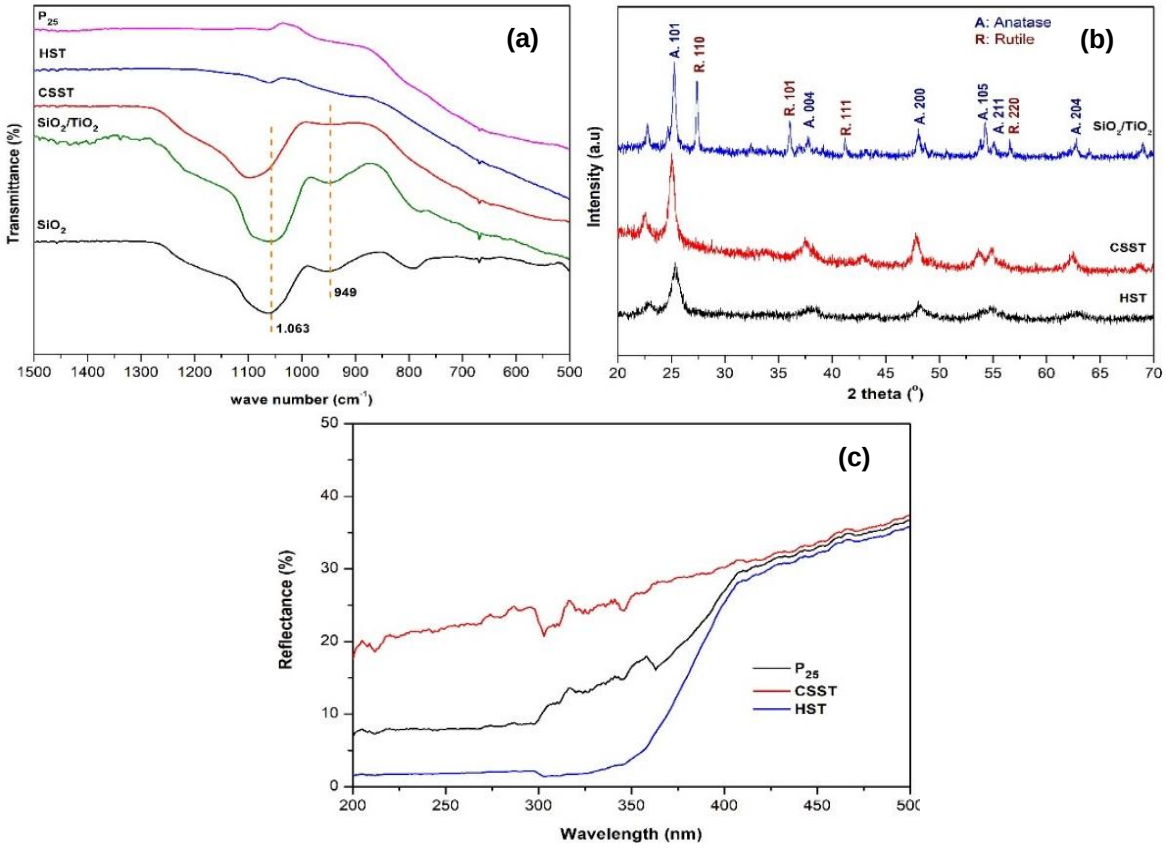

Figure 2. P_{25}, CSST, and HST profile: (**a**) FTIR, (**b**) XRD, (**c**) UV-vis diffuse reflectance.

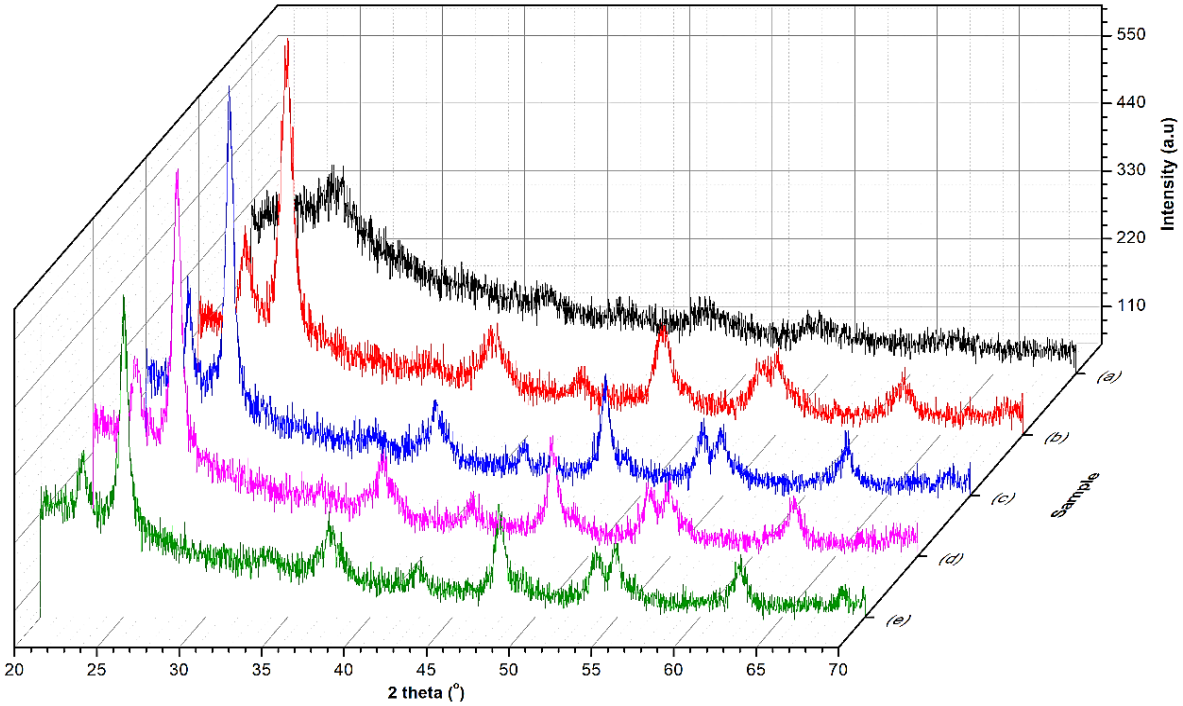

Figure 3. The XRD profile of CSST for different annealing times: (**a**) 0 hours (without annealing time/control); (**b**) 1 hour; (**c**) 2 hours; (**d**) 4 hours; and (**e**) 6 hours.

On the other hand, **Figure 2.c** shows the UV-Vis diffuse reflectance spectra. The edge reflectance at 400 nm supports the morphological features of CSST and HST, suggesting the presence of the anatase profile of TiO_2. This observation is consistent with previous findings on a core-shell structure of TiO_2(rod)-SiO_2 (Wahyuni et al., 2018; Wahyuni et al., 2017). The presence of a cavity can extend the

wavelength path (Lei et al., 2014), which makes the HST has a lower reflectance than P_{25} and CSST at a wavelength of 200-400 nm, which is 3.04 eV related to the band gap of HST.

Effect of Annealing and Etching Time

The crystal structure of HST anatase with the annealing process was slowed down by Si-O-Ti in CSST, thus requiring more high temperatures than the pristine (Zheng et al., 2018). The construction of the anatase crystal structure began at one hour of annealing and was steady after six hours (**Figure 3**). The peak intensity of 101 at 25 degrees of 2θ was the highest at 2 hours and decreased after 4 hours of annealing. The annealing time affects the crystal size and microstrain accessed by Williamson-Hall (W-H) plotting (**Table 1**). The W-H analysis used the XRD profile by linear plotting of βcosθ vs sinθ, as following Equation 2 (Kibasomba et al., 2018).

$$\beta\cos\theta = K\lambda/D + 4\varepsilon\sin\theta \quad (2)$$

Where β is the full-width-at-half-maximum (FWHM) of the i-th peak, θ is the angle from the i-th peak radian found, K is the instrument alignment constant with a magnitude of 0.94, and λ is the wavelength of the X-ray source of Cu K_α at 1.54 Å, and ε is the microstrain (Rehani et al., 2006).

The W-H analysis involved creating a graph where βcosθ was plotted on the y-axis and 4sinθ on the x-axis. From this graph, a linear regression was determined, and the resulting intercept and slope were utilized to calculate the crystallite size (D) and microstrain (ε). **Table 1** shows the optimum crystal size and microstrain of HST anatase at 20.54 nm and 3.42, respectively, after 2 hours of annealing. Crystal size and microstrain decreased after a longer annealing process. This affects the reduced surface area and oxygen content (John et al., 2021). From **Table 1**, etching time affected the crystallite size and microstrain of HST. The crystallite size of HST was decreased in a longer time of etching, except in 7 hours of etching were enhance the microstrain of HST. The investigation of the SiO_2 etching process by an energy-dispersive X-ray spectrometer is shown in **Figure 4.a**.

The optimum time for removing the SiO_2 core using 2.5 M NaOH solution was 5 hours (**Figure 4.b**). The etching process via sonication after 5 hours was steady at less than 2% mass percent of Si. The etching time has improved the crystal size and microstrain HST (**Table 1**). The XRD profile shows the crystallite size of TiO_2 anatase CSST shrinks after the etching process. Etching for 5 hours constructed a crystallite size of 12.66 nm, with the lowest microstrain of 1.84. The etching via sonication for 5 hours is the optimum time to construct anatase TiO_2 of HST via sonication.

Table 1. Profile of the W-H plotting

Anneal time (h)	D^a (nm)	ε^a	Etching time (h)	D^e (nm)	ε^e
1	9.53	0.34	1	20.54	3.42
2	20.54	3.42	3	12.58	2.26
4	15.47	2.35	5	12.66	1.84
6	13.92	0.65	7	11.22	2.97

D^a, D^e: crystallite size of aneal time & etching time; ε^a, ε^e: microstrain of annealing time & etching time

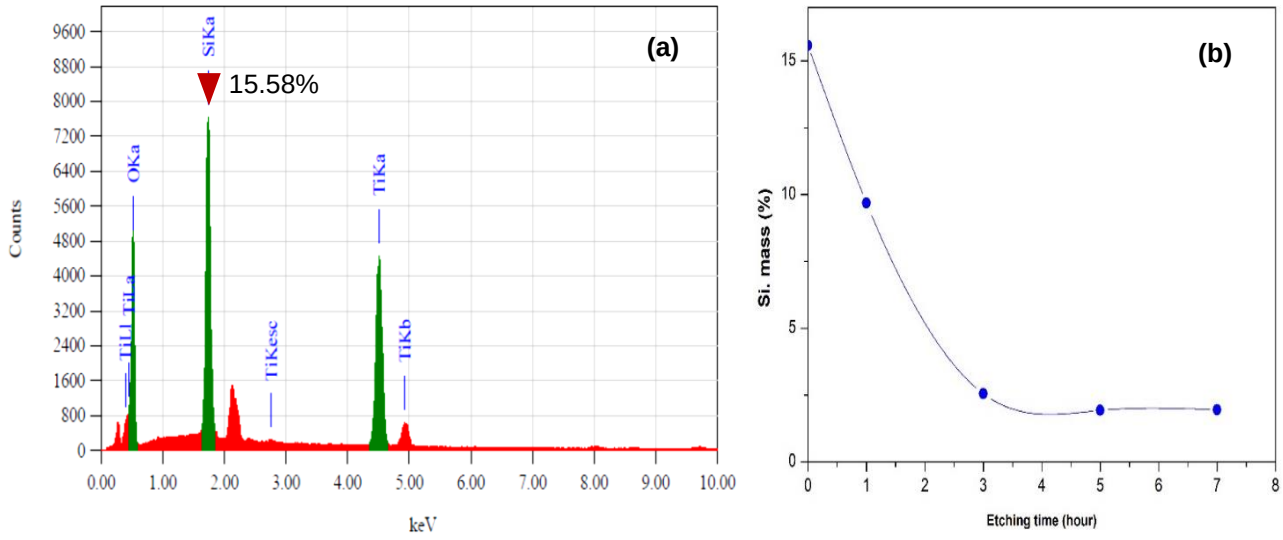

Figure 4. (**a**). EDX spectra of CSST, (**b**) effect of etching time on percent Si mass.

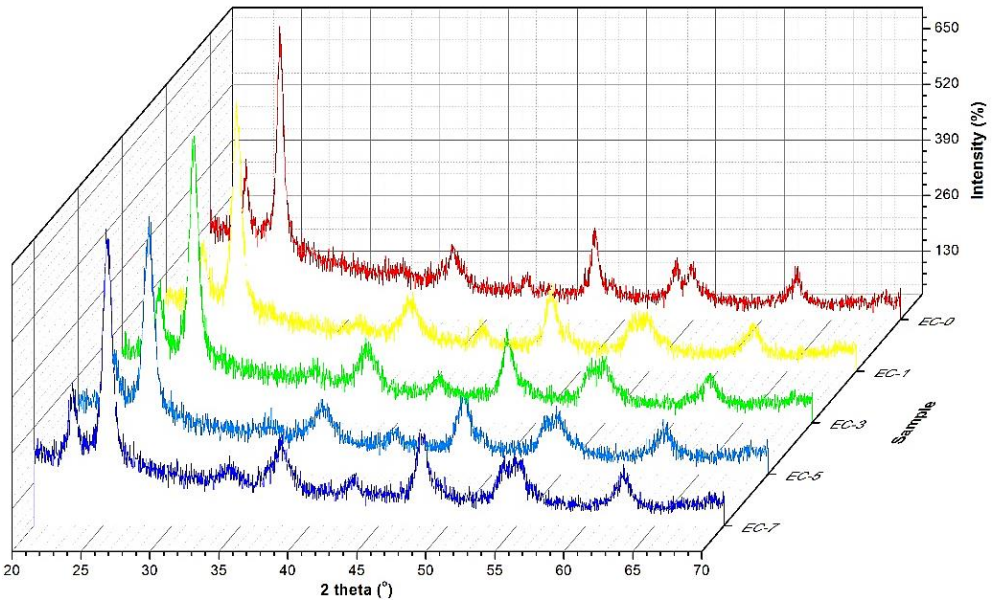

Figure 5. XRD profile of etching time of HST

Based on the XRD profile (**Figure 5**) from the difference in etching time, the HST anatase peaks were the same as CSST. The longer time of the etching process does not affect the HST crystal phase but has improved the crystallite size and microstrain.

Photocatalytic Activity

The photocatalytic of iodide ion (I^-) from KI solution by HST has changed the clear solution to bright yellow which is indicative of the formation of I_3^-. The photocatalytic activity of HST was evaluated by the I_3^- formation from the oxidation of I^- to I_2 in the excess iodide, following the reaction as shown in Equation 3-7 (Adachi et al., 2003; Watanabe et al., 2019). While the involvement of HST refers to the theory and principle of the nanostructure-TiO_2 universal photocatalyst, namely the indirect photocatalytic mechanism (Long et al., 2017). The concentration of I_3^- from photooxidation with HST 2 catalyst at 60 min of 10.2×10^{-6} M is higher than HST 4, 6, and 1 (**Figure 6**).

$$I^-_{(aq)} + h\nu\ (UV) \rightarrow I^{-*} \quad (3)$$

$$I^{-*} \rightarrow [I + e^-]_{(aq)} \quad (4)$$

$$[I + e^-]_{(aq)} + K^+_{(aq)} \rightarrow I_{(aq)} + K_{(aq)} \quad (5)$$

$$I_{(aq)} + I^-_{(aq)} \leftrightarrow I^-_2 \quad (6)$$

$$I_{(aq)} + I^-_{2\,(aq)} \rightarrow I^-_{3(aq)} \quad (7)$$

At the same irradiation time, HST 4, 6, and 1 produced I_3^- concentrations of 9.08×10^{-6}, 8.85×10^{-6}, and 6.73×10^{-6} M, respectively. Crystallite size and microstrain have affected the photooxidation of KI. The photocatalytic activity showed that the large crystallite size and microstrain of HST enhance the concentrations of I_3^-. The I_3^- was produced after the KI

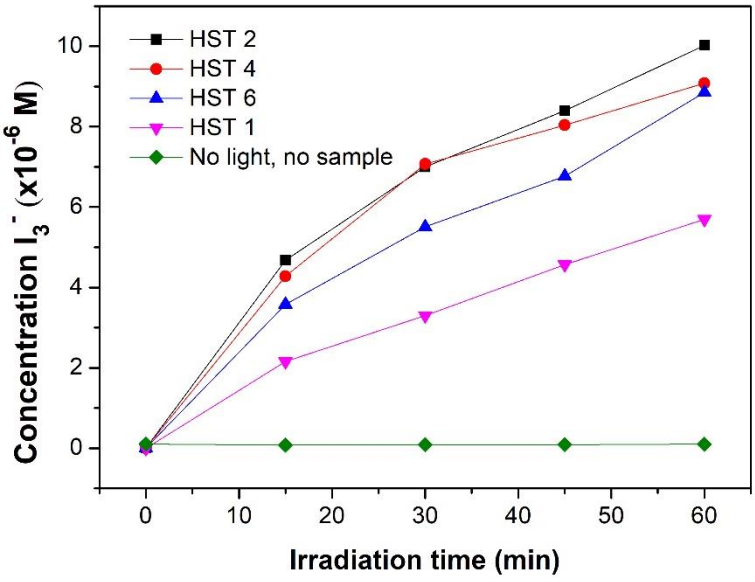

Figure 6. Photocatalytic activity (I_3^- concentration) of the HST annealed at altered times

solution and the catalyst were stirred under UV light. Overall, we have shown that morphology engineering through the HST formation has resulted in improved photocatalytic performance. A similar finding of improved performance of the photocatalyst due to morphological changes has also been observed for silver phosphate photocatalysts (Sulaeman et al., 2022). As a result, there is a growing interest in conducting further research on shaping the morphology of photocatalysts.

CONCLUSIONS

Hollow sphere TiO_2 (HST) has been successfully synthesized by the sol-gel method through the formation of a core-shell silica@titania (CSST). The anatase crystal of HST was constructed at 1 hour of annealing at 900 °C. Meanwhile, the removal of the SiO_2 core to form HST was obtained after 3 hours of the etching process with 2.5 M NaOH solution. Synthesis from this method fabricates HST with a particle size of ~90 nm, shell thickness of ~26 nm, and cavity size of ~45 nm. The synthesis of HST with different annealing and etching times has improved the crystallite size and microstrain. The large crystallite size and microstrain can increase the photocatalytic activity of photooxidation of I^-.

ACKNOWLEDGMENTS

The authors gratefully acknowledge financial support by Universitas Gadjah Mada RTA Grant 2022 (5722/UN1.P.III/Dit-Lit/PT.01.05/2022).

REFERENCES

Adachi, M., Murata, Y., Okada, I., & Yoshikawa, S. (2003). Formation of titania nanotubes and applications for dye-sensitized solar cells. *Journal of The Electrochemical Society*, *150*(8), G488. https://doi.org/10.1149/1.1589763

Chang, M., Song, Y., Chen, J., Cui, L., Sheng, Y., Shi, Z., & Zou, H. (2017). $SiO_2@TiO_2:Eu^{3+}$ and its derivatives: Design, synthesis, and properties. *Crystal Growth and Design*, *17*(12), 6486–6497. https://doi.org/10.1021/acs.cgd.7b01149

Chen, Z. H., Kim, C., Zeng, X. B., Hwang, S. H., Jang, J., & Ungar, G. (2012). Characterizing size and porosity of hollow nanoparticles: SAXS, SANS, TEM, DLS, and adsorption isotherms compared. *Langmuir*, *28*(43), 15350–15361. https://doi.org/10.1021/la302236u

Choi, M., Kim, C., Ok Jeon, S., Soo Yook, K., Yeob Lee, J., & Jang, J. (2011). Synthesis of titania embedded silica hollow nanospheres via sonication mediated etching and re-deposition. *Chemical Communications*, *47*(25), 7092–7094. https://doi.org/10.1039/c1cc11185j

Doubi, Y., Hartiti, B., Hicham, L., Fadili, S., Batan, A., Tahri, M., Belfhaili, A., & Thevnin, P. (2019). Effect of annealing time on structural and optical proprieties of TiO_2 thin films elaborated by spray pyrolysis technique for future gas sensor application. *Materials Today: Proceedings*, *30*, 823–827. https://doi.org/10.1016/j.matpr.2020.04.186

Fang, B., Xing, Z., Sun, D., Li, Z., & Zhou, W. (2022). Hollow semiconductor photocatalysts for solar energy conversion. *Advanced Powder Materials*, *1*(2), 100021. https://doi.org/10.1016/j.apmate.2021.11.008

Jafarzadeh, M., Sipaut, C. S., Dayou, J., & Mansa, R. F. (2016). Recent progresses in solar cells: Insight into hollow micro/nano–structures. *Renewable and Sustainable Energy Reviews*, *64*, 543–568. https://doi.org/10.1016/j.rser.2016.06.028

Jeng, M. J., Wung, Y. L., Chang, L. B., & Chow, L. (2013). Particle size effects of TiO_2 layers on the solar efficiency of dye-sensitized solar cells. *International Journal of Photoenergy*, *2013*. https://doi.org/10.1155/2013/563897

John, K. I., Adenle, A. A., Adeleye, A. T., Onyia, I. P., Amune-Matthews, C., & Omorogie, M. O. (2021). Unravelling the effect of crystal dislocation density and microstrain of titanium dioxide nanoparticles on tetracycline removal performance. *Chemical Physics Letters*, *776*(May). https://doi.org/10.1016/j.cplett.2021.138725

Kanjana, N., Maiaugree, W., Poolcharuansin, P., & Laokul, P. (2020). Size controllable synthesis and photocatalytic performance of mesoporous TiO_2 hollow spheres. *Journal of Materials Science and Technology*, *48*, 105–113. https://doi.org/10.1016/j.jmst.2020.03.013

Kibasomba, P. M., Dhlamini, S., Maaza, M., Liu, C. P., Rashad, M. M., Rayan, D. A., & Mwakikunga, B. W. (2018). Strain and grain size of TiO_2 nanoparticles from TEM, raman spectroscopy and XRD: The revisiting of the Williamson-Hall plot method. *Results in Physics*, *9*, 628–635. https://doi.org/10.1016/j.rinp.2018.03.008

Kim, C., Choi, M., & Jang, J. (2010). Nitrogen-doped SiO_2/TiO_2 core/shell nanoparticles as highly efficient visible light photocatalyst. *Catalysis Communications*, *11*(5), 378–382. https://doi.org/10.1016/j.catcom.2009.11.005

Lee, J., Kong, S., Kim, W., & Kim, J. (2007). Preparation and characterization of SiO_2/TiO_2 core-shell particles with controlled shell thickness. *Materials Chemistry and Physics*, *106*, 39–44. https://doi.org/10.1016/j.matchemphys.2007.05.019

Lei, B. X., Zhang, P., Qiao, H. K., Zheng, X. F., Hu, Y. S., Huang, G. L., Sun, W., Sun, Z. F., & Zhang, X. X. (2014). A facile template-free route for synthesis of anatase TiO_2 hollow spheres for dye-sensitized solar cells. *Electrochimica Acta*, *143*, 129–134. https://doi.org/10.1016/

j.electacta.2014.07.106

Li, S., Chen, J., Zheng, F., Li, Y., & Huang, F. (2013). Synthesis of the double-shell anatase-rutile TiO_2 hollow spheres with enhanced photocatalytic activity. *Nanoscale*, *5*(24), 12150–12155. https://doi.org/10.1039/c3nr04043g

Li, X., Leng, W., & Cao, C. (2013). Quantitatively understanding the mechanism of highly enhanced regenerated dye sensitized photooxidation of arsenite over nanostructured TiO_2 electrodes under visible light by I-. *Journal of Electroanalytical Chemistry*, *703*, 70–79. https://doi.org/10.1016/j.jelechem.2013.05.025

Liao, J. Y., He, J. W., Xu, H., Kuang, D. Bin, & Su, C. Y. (2012). Effect of TiO_2 morphology on photovoltaic performance of dye-sensitized solar cells: Nanoparticles, nanofibers, hierarchical spheres and ellipsoid spheres. *Journal of Materials Chemistry*, *22*(16), 7910–7918. https://doi.org/10.1039/c2jm16148f

Long, J. J., Liu, B., Wang, G. F., & Shi, W. (2017). Photocatalitic stripping of fixed reactive red X-3B dye from cotton with nano-TiO2/UV system. *Journal of Cleaner Production*, *165*, 788–800. https://doi.org/10.1016/j.jclepro.2017.07.149

Lyu, J., Zhou, L., Shao, J., Zhou, Z., Gao, J., Dong, Y., Wang, Z., & Li, J. (2020). TiO_2 hollow heterophase junction with enhanced pollutant adsorption, light harvesting, and charge separation for photocatalytic degradation of volatile organic compounds. *Chemical Engineering Journal*, *391*(November 2019), 1–8. https://doi.org/10.1016/j.cej.2019.123602

Meier, M., Ungerer, J., Klinge, M., & Nirschl, H. (2018). Synthesis of nanometric silica particles via a modified Stöber synthesis route. *Colloids and Surface A*, *538*(September 2017), 559–564.

Oh, W. K., Kim, S., Choi, M., Kim, C., Jeong, Y. S., Cho, B. R., Hahn, J. S., & Jang, J. (2010). Cellular uptake, cytotoxicity, and innate immune response of silica-Titania hollow nanoparticles based on size and surface functionality. *ACS Nano*, *4*(9), 5301–5313. https://doi.org/10.1021/nn100561e

Pavasupree, S., Ngamsinlapasathian, S., Nakajima, M., Suzuki, Y., & Yoshikawa, S. (2006). Synthesis, characterization, photocatalytic activity and dye-sensitized solar cell performance of nanorods/nanoparticles TiO_2 with mesoporous structure. *Journal of Photochemistry and Photobiology A: Chemistry*, *184*(1–2), 163–169. https://doi.org/10.1016/j.jphotochem.2006.04.010

Rehani, B. R., Joshi, P. B., Lad, K. N., & Pratap, A. (2006). Crystallite size estimation of elemental and composite silver nano-powders using XRD principles. *Indian Journal of Pure and Applied Physics*, *44*(2), 157–161.

Shakeel, M., Pandey, A. K., & Abd, N. (2017). Advancements in the development of TiO_2 photoanodes and its fabrication methods for dye sensitized solar cell (DSSC) applications. A review. *Renewable and Sustainable Energy Reviews*, *77*(March), 89–108. https://doi.org/10.1016/j.rser.2017.03.129

Stober, W. & Fink, A. (1968). Controlled growth of monodisperse silica spheres in the micron size range 1. *Journal of Colloid and Interface Science*, *26*, 62–69.

Sulaeman, U., Afifah, K., Diastuti, H., & Yin, S., 2022. The enrichment of silver ions in Ag_3PO_4 through the morphology changes and their photocatalytic activities. *Molekul*, *17*(1), 10-18. https://doi.org/10.20884/1.jm.2022.17.1.5606

Thejas, K. K., Supin, K. K., Akshay, V. R., Arun, B., Mandal, G., Chanda, A., & Vasundhara, M. (2022). Effect of annealing time on structural, optical and magnetic properties of TiO_2 nanoparticles. *Optical Materials Journal*, *134*(July), 1–8.

Tighineanu, A., Ruff, T., Albu, S., Hahn, R., & Schmuki, P. (2010). Conductivity of TiO_2 nanotubes: Influence of annealing time and temperature. *Chemical Physics Letters*, *494*(4–6), 260–263. https://doi.org/10.1016/j.cplett.2010.06.022

Tsai, M. C., Lee, J. Y., Chang, Y. C., Yang, M. H., Chen, T. T., Chang, I. C., Lee, P. C., Chiu, H. T., Lee, R. K., & Lee, C. Y. (2014). Scattering resonance enhanced dye absorption of dye sensitized solar cells at optimized hollow structure size. *Journal of Power Sources*, *268*, 1–6. https://doi.org/10.1016/j.jpowsour.2014.06.015

Wahyuni, S., Kunarti, E.S., Swasono, R.T., & Kartini, I. (2017). Study on the properties and photoactivity of TiO_2(nanorod)-SiO_2 synthesized by sonication technique. *Oriental Journal of Chemistry*, *33*(1), .249. https://doi.org/10.13005/ojc/330129

Wahyuni, S., Kunarti, E.S., Swasono, R.T., & Kartini, I. (2018). Characterization and photocatalytic activity of TiO_2 (rod)-SiO_2-polyaniline nanocomposite. *Indonesian Journal of Chemistry*, *18*(2), 321-330. https://doi.org/10.22146/ijc.22550

Wang, D., Tan, Y., Xu, H., Wang, X., Yu, L., Xiao, Z., & Wang, J. (2019). A tough and fluorescent dual nanocomposite hydrogel based on SiO_2@TiO_2 core-shell nanoparticles. *Applied Surface Science*, *468*(August 2018), 588–595. https://doi.org/10.1016/j.apsusc.2018.10.208

Wang, X., Li, Z., Shi, J., & Yu, Y. (2014). One-Dimensional Titanium Dioxide Nanomaterials : Nanowires ,. *Chemical Reviews*, *114*, 9346–9384. https://doi.org/10.1021/cr400633s

Watanabe, K., Matsuda, S., Cuevas, C. A., Saiz-Lopez, A., Yabushita, A., & Nakano, Y. (2019). Experimental determination of the photooxidation of aqueous I^- as a source of atmospheric I_2. *ACS Earth and Space Chemistry*, *3*(4), 669–679. https://doi.org/10.1021/acsearthspacechem.9b00007

Yun, J., Hwang, S. H., & Jang, J. (2015). Fabrication of Au@Ag Core/shell nanoparticles decorated TiO_2 hollow structure for efficient light-harvesting in dye-sensitized solar cells. *ACS Applied Materials & Interfaces*, *7*, 2055−2063. https://doi.org/10.1021/am508065n

Zheng, H., Svengren, H., Huang, Z., Yang, Z., Zou, X., & Johnsson, M. (2018). Hollow titania spheres loaded with noble metal nanoparticles for photocatalytic water oxidation. *Microporous and Mesoporous Materials*, *264*(July 2017), 147–150. https://doi.org/10.1016/j.micromeso.2018.01.012

Zhu, L., Liu, K., Li, H., Sun, Y., & Qiu, M. (2013). Solvothermal synthesis of mesoporous TiO2 microspheres and their excellent photocatalytic performance under simulated sunlight irradiation. *Solid State Sciences*, *20*, 8–14. https://doi.org/10.1016/j.solidstatesciences.2013.02.026